

## EXAFS studies of the local environment of lead and selenium atoms in $\text{PbTe}_{1-x}\text{Se}_x$ solid solutions

A. I. Lebedev, I. A. Sluchinskaya, and V. N. Demin

*M. V. Lomonosov Moscow State University, 119899 Moscow, Russia*

I. Munro

*Daresbury Laboratory, Warrington WA4 4AD, UK*

(Submitted December 11, 1998; resubmitted January 20, 1999)

Fiz. Tverd. Tela (St. Petersburg) **41**, 1394–1402 (August 1999)

EXAFS spectroscopy is used to study the local environment of lead and selenium atoms in  $\text{PbTe}_{1-x}\text{Se}_x$  solid solutions. In addition to a bimodal distribution of the bond lengths in the first-coordination sphere, an unusually large value of the Debye–Waller factors for the Pb–Pb interatomic distances (second-coordination sphere) and a substantial deviation of this value from Vegard’s law are observed. Monte Carlo calculations show that these observations are related to the complicated structure of the distribution function for Pb–Pb distances. It is found that the number of Se–Se pairs in the second-coordination sphere exceeds the statistical value, which indicates that chemical factors play an important role in the structure of the solid solutions. The contribution of chemical factors to the enthalpy of mixing of the solid solution is estimated ( $\approx 0.5$  kcal/mole) and this value is shown to be comparable to the deformation contribution. © 1999 American Institute of Physics. [S1063-7834(99)00908-9]

Knowledge of the true structure of solid solutions, i.e., the local displacements of atoms from their ideal lattice sites and the deviations in the distributions of the atoms from statistical distributions, is needed to understand the physical properties of these crystals. EXAFS spectroscopy is now widely used for studying the structure of solid solutions.

EXAFS studies of solid solutions of III-V and II-VI semiconductors having the sphalerite structure<sup>1–6</sup> have revealed a bimodal distribution of the bond lengths in the first-coordination sphere. This implied that the local structure of the solid solutions should, most likely, be described in the approximation of fixed chemical bond lengths proposed by Bragg and Pauling, rather than in the approximation of a virtual crystal. Up to now, solid solutions of IV-VI semiconductors having the rock salt (NaCl) structure have been studied by EXAFS only to examine the locations of the noncentral impurities;<sup>7–10</sup> no systematic investigations of the local structure have been made for these solid solutions that contain no noncentral impurities.

In this paper we present results from a study of the local structure of  $\text{PbTe}_{1-x}\text{Se}_x$  solid solutions by EXAFS spectroscopy. These solid solutions are of great interest in connection with their use for creating IR optoelectronic devices based on heterostructures with matching crystal-lattice parameter. PbTe and PbSe form a continuous series of solid solutions over the entire range of compositions. The periods of the crystal lattices in the initial binary compounds are 6.460 and 6.126 Å at 300 K, i.e., this solid solution is characterized by a rather large relative difference (slightly larger than 5%) in the interatomic distances. In addition, this solid solution was of interest to us because, in it, for  $x \approx 0.25$ , the lattice was found to be “softest” with respect to the appearance of a ferroelectric phase when tin atoms are introduced.<sup>11</sup>

### 1. EXPERIMENTAL TECHNIQUE

Samples of  $\text{PbTe}_{1-x}\text{Se}_x$  solid solution with  $x = 0.1, 0.25, 0.5,$  and  $0.75$  were obtained by melting stoichiometric compositions of the binary compounds PbTe and PbSe together in evacuated quartz vials with subsequent homogenizing annealing at 720 °C for 170 h. According to x-ray measurements, the samples were single-phase. Immediately before the EXAFS measurements, the alloys were ground to a powder, sifted through a mesh, and deposited on a scotch tape. An optimum thickness of the absorbing layer for taking spectra was obtained by multiple layering (usually 8 layers) of the type.

The EXAFS spectra were studied at station 7.1 of the synchrotron radiation source at the Daresbury Laboratory (Great Britain) with an electron energy of 2 GeV and a maximum beam current of 230 mA. Measurements were made at the *K* absorption edge of Se (12658 eV) and the *L* absorption edge of Pb (13055 eV) at 80 K in transmission geometry. The synchrotron radiation was monochromatized by a two-crystal Si(111) monochromator. The intensities of the radiation incident on ( $I_0$ ) and transmitted through ( $I_t$ ) the sample were recorded by ionization chambers filled with He + Ar mixtures with compositions such that 20 and 80% of the x radiation, respectively, was absorbed. Contamination of the radiation output from the monochromator by higher harmonics could be neglected for the energy range employed in these experiments.

The resulting spectra were analyzed in the usual way.<sup>12</sup> After subtraction of the background absorption of the radiation by other atoms, the monotonic part  $\mu_{x_0}(E)$  of the ab-

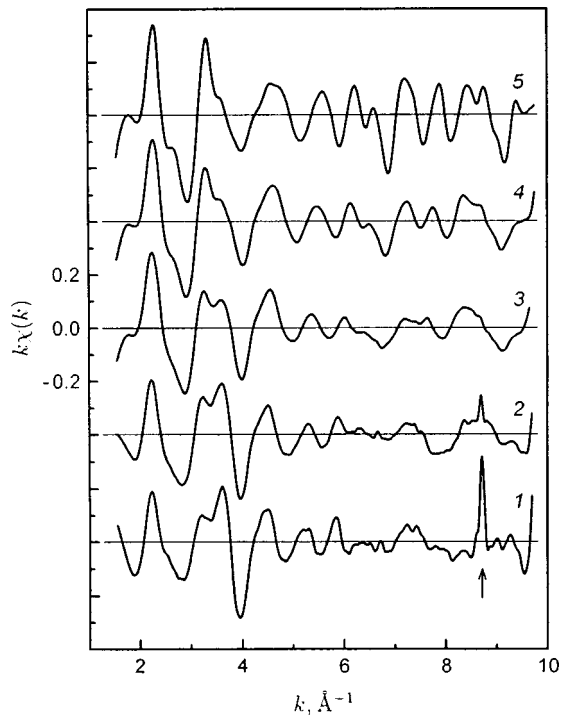


FIG. 1.  $k\chi(k)$  for samples of  $\text{PbTe}_{1-x}\text{Se}_x$  at the  $K$  absorption edge of Se.  $x$ : 1 — 0, 2 — 0.1, 3 — 0.25, 4 — 0.5, 5 — 1. The arrow denotes the location of the glitches.

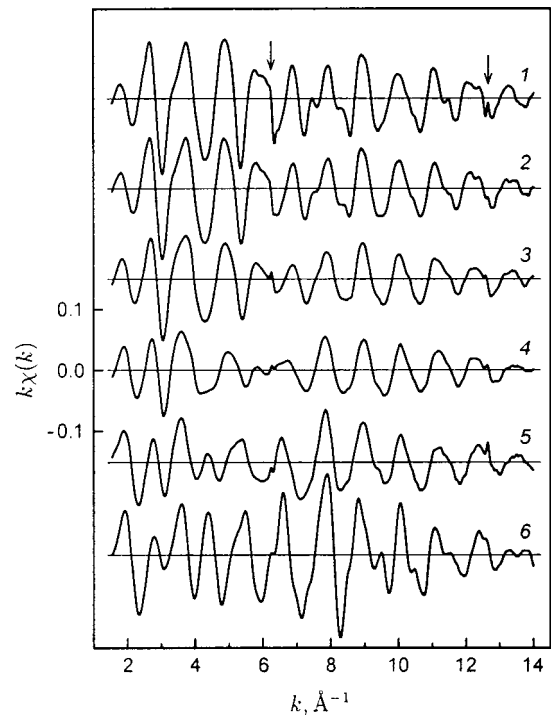


FIG. 2.  $k\chi(k)$  for samples of  $\text{PbTe}_{1-x}\text{Se}_x$  at the  $L_{\text{III}}$  absorption edge of Pb.  $x$ : 1 — 0, 2 — 0.1, 3 — 0.25, 4 — 0.5, 5 — 0.75, 6 — 1. The arrows indicate the locations of glitches.

sorption was separated from the transmission curves  $\mu x(E) = \ln(I_0/I_t)$  (here  $E$  is the energy of the radiation) by curve fitting and the EXAFS function  $\chi = (\mu x - \mu x_0)/\mu x_0$  was calculated as a function of the photoelectron wave vector  $k = [2m(E - E_0)/\hbar^2]^{1/2}$ . The origin for the photoelectron energy  $E_0$  was taken to be the energy corresponding to the inflection point in the absorption edge. The jump  $\mu x$  at the absorption edge varied over 0.08–1.4. At least two spectra were taken for each sample.

When multiple scattering effects are neglected, information on the local environment of the central atom, i.e., the distances  $R_j$ , coordination numbers  $N_j$ , and Debye-Waller factors  $\sigma_j^2$ , for each  $j$ th coordination sphere enters the EXAFS function as follows:<sup>12</sup>

$$\chi(k) = \frac{1}{k} \sum_j \frac{N_j S_0^2}{R_j^2} f(k) \exp[-2R_j/\lambda(k)] - 2k^2 \sigma_j^2 \sin[2kR_j + \psi(k)].$$

Besides the structural parameters characterizing the local environment, this equation includes the amplitude  $f(k)$ , the sum of the backscatter phase and the phase of the central atom  $\psi(k)$ , the photoelectron mean-free-path  $\lambda(k)$ , and a parameter  $S_0^2$ , which accounts for many-electron and inelastic effects in the central and scattering atoms. The functions  $f(k)$ ,  $\psi(k)$ , and  $\lambda(k)$  were calculated using the FEFF5 program.<sup>13</sup>

The information of interest to us for the first-coordination spheres was extracted from the experimental  $\chi(k)$  curves with the aid of the forward and inverse Fourier transforms using Hemming windows. Quantitative values of

the parameters  $R_j$ ,  $N_j$ , and  $\sigma_j^2$  were found by minimizing the root-mean-square deviation between the experimental and calculated  $k\chi(k)$  curves using a modified Levenberg–Marquardt algorithm. Besides these parameters, the shift in the zero on the energy scale  $dE_0$  was varied simultaneously. The number of varied parameters (8–9) was usually half the number of independent parameters in the data ( $2\Delta k \Delta R/\pi = 12\text{--}20$ , where  $\Delta k$  and  $\Delta R$  are the regions for discrimination of the data under Fourier filtration in  $k$  and  $R$  space<sup>12</sup>). The accuracy with which the parameters was determined was established from the covariant matrix. The errors reported here correspond to the standard deviation. In order to enhance the accuracy, it was assumed that the correction energy  $dE_0$  is the same for all the coordination spheres, while the coordination numbers correspond to the known coordination numbers in an fcc lattice.

## 2. EXPERIMENTAL RESULTS

Figure 1 shows typical experimental  $k\chi(k)$  curves obtained at the  $K$  absorption edge of Se for samples of  $\text{PbTe}_{1-x}\text{Se}_x$  and  $\text{PbSe}$ . The range of wave numbers for these data is bounded above by  $k \approx 9.7 \text{ \AA}^{-1}$  because of the closeness of the  $L_{\text{III}}$  absorption edge of lead. Figure 2 shows plots of  $k\chi(k)$  for samples of  $\text{PbTe}_{1-x}\text{Se}_x$ ,  $\text{PbTe}$ , and  $\text{PbSe}$  at the  $L_{\text{III}}$  absorption edge of Pb. The sharp jumps in the curves indicated by arrows in Figs. 1 ( $k \approx 8.7 \text{ \AA}^{-1}$ ) and 2 ( $k \approx 6.2$  and  $12.7 \text{ \AA}^{-1}$ ), the so-called glitches, are not related to properties of the samples, but to those of the monochromator. After the glitches were removed, the data were analyzed by the method described in the previous section.

TABLE I. Experimentally determined local concentrations of Se atoms surrounding Se.

$x$	0.1	0.25	0.5	0.75	1.0
$N_{\text{Se-Se}}/12$	$0.34 \pm 0.04$	$0.45 \pm 0.03$	$0.60 \pm 0.02$	$0.78 \pm 0.01$	$0.96 \pm 0.02$

In processing the data, we have restricted ourselves to finding the parameters for the first two coordination spheres. In analyzing the data at the absorption edge of Pb, it was noted that the lead atoms in the first-coordination sphere are surrounded by six atoms of two kinds (Se and Te). Here each pair (Pb–Te, Pb–Se) is described by its own set of structural parameters ( $R_j$ ,  $N_j$ ,  $\sigma_j^2$ ). The second-coordination sphere consists of 12 lead atoms which, we have assumed lie at the same distance.<sup>a)</sup> In order to reduce the number of variable parameters, the relative contributions of the Pb–Te and Pb–Se pairs in the  $\chi(k)$  curves were calculated using the known chemical compositions of the samples and the relative contributions of the first- and second-coordination spheres, in accordance with their coordination numbers. The complete set of parameters characterizing the nearest neighbors of the lead atoms was characterized by 8 parameters.

In analyzing the data taken at the Se absorption edge, we assumed that the first-coordination sphere of the selenium always consists of 6 lead atoms, while the second-coordination sphere can contain either Se or Te atoms. Here the number of Se and Te atoms in the second-coordination sphere can differ from the statistical number because of short-range order in the solid solution. Thus, the analysis was done both in the approximation of a statistical distribution of chalcogenide atoms in the lattice and taking the possibility of short-range order into account.

In the case of a statistical distribution of chalcogenide atoms, the problem was limited to finding a set of 8 parameters characterizing the short-range order of the Se atoms in the solid solution.<sup>b)</sup>

In order to account for the possible deviation from a statistical distribution of the chalcogenide atoms in the second-coordination sphere of Se, yet another variational parameter was introduced,  $N_{\text{Se-Se}}$ , the number of Se atoms in the second-coordination sphere of an Se atom. Here it was assumed that the total number of atoms in the second-coordination sphere was always equal to 12.

Taking the possibility of short-range order into account when processing the data ensured a considerably better agreement between the experimental and theoretical  $k\chi(k)$  curves than for a random distribution of atoms in the lattice. The values of  $N_{\text{Se-Se}}$  which we obtained (see Table I) indicate a distinct short-range order, specifically, Se atoms being surrounded in the second-coordination sphere by atoms of the same type. This is consistent with a study of the thermodynamic properties of the PbTe–PbSe system.<sup>14</sup>

Figures 3 and 4 contain plots the interatomic distances and Debye–Waller factors as functions of the composition  $x$  for Pb–Te and Pb–Se bonds obtained by analyzing data from both absorption edges.<sup>c)</sup> Despite the rather large errors in determining the Pb–Se distances in samples with a low selenium content, the distances obtained at both absorption

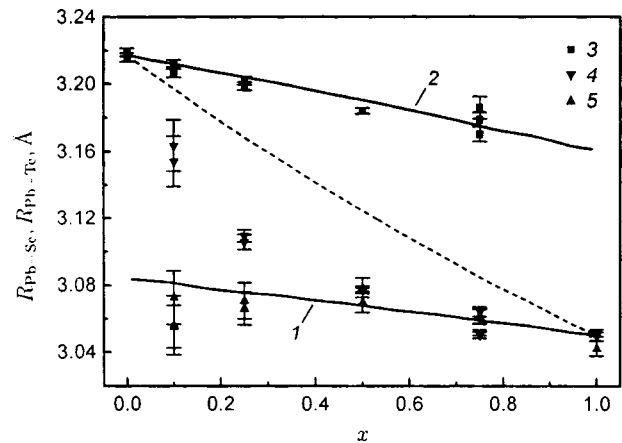


FIG. 3. Average interatomic Pb–Se (1) and Pb–Te (2) distances as functions of the composition  $x$  of  $\text{PbTe}_{1-x}\text{Se}_x$  solid solutions. The points indicate the bond lengths of: 3 — Pb–Te, 4 — Pb–Se, 5 — Se–Pb. The smooth curves are from a Monte Carlo model calculation and the dashed curve is the average interatomic distance (half the lattice parameter).

edges are in agreement. As Fig. 3 implies, the distribution of the interatomic bond lengths in  $\text{PbTe}_{1-x}\text{Se}_x$  solid solutions has a distinct bimodal character. The Debye–Waller factor depends on  $x$  differently for the Pb–Te and Pb–Se bonds (Fig. 4): while  $\sigma_{\text{Pb-Te}}^2$  is essentially independent of the composition,  $\sigma_{\text{Pb-Se}}^2$  has a maximum near  $x=0.5$ . Nevertheless,  $\sigma^2$  is less than  $0.01 \text{ \AA}^2$  for both bonds.

Figures 5 and 6 contain plots of the interatomic distances and Debye–Waller factors as functions of the composition parameter for Pb–Pb atom pairs located in the second-coordination sphere with respect to one another, and Figs. 7 and 8, similar curves for Se–chalcogen atom pairs assuming short-range order. These figures imply that the experimental dependence of the Pb–Pb distance deviates significantly from a Vegard law, while the Se–chalcogen pairs follow Vegard’s law much better.

The dependences of the Debye–Waller factors for Pb–Pb and Se–chalcogen atom pairs on  $x$  are qualitatively analogous, although they differ quantitatively. In these data, it is

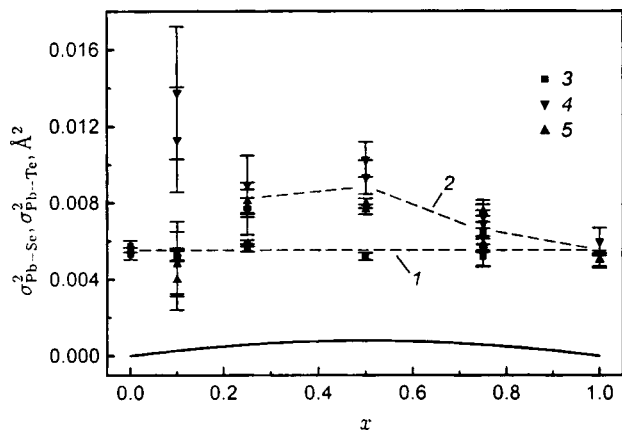


FIG. 4. The Debye–Waller factors for Pb–Te (1) and Pb–Se (2) bonds as functions of the composition  $x$  of  $\text{PbTe}_{1-x}\text{Se}_x$  solid solutions. The points denote data for the bonds: 3 — Pb–Te, 4 — Se–Pb, 5 — Pb–Se. The smooth curve is the static contribution to the Debye–Waller factor calculated by a Monte Carlo method. (The curves for both bonds essentially overlap.)

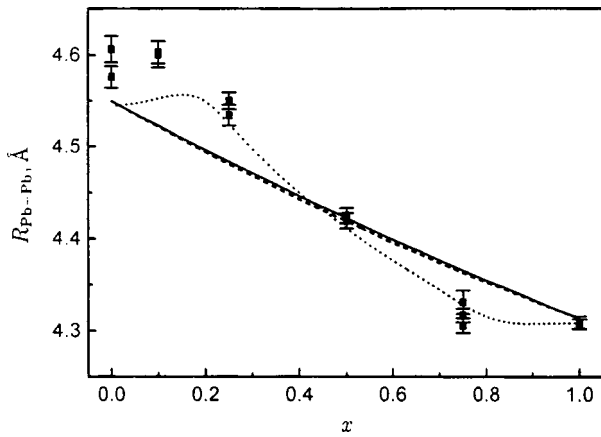


FIG. 5. The Pb–Pb interatomic distance as a function of the composition  $x$  of  $\text{PbTe}_{1-x}\text{Se}_x$  solid solutions. The points are experimental data. The smooth curve was calculated by a Monte Carlo method, the dashed curve is the average interatomic distance, and the dotted curve is the result of an analysis for the model  $\chi(k)$  curves.

noteworthy that the Debye–Waller factors for Pb–Pb pairs reach a maximum near  $x \approx 0.25$ , while these values are unexpectedly large (up to  $0.05 \text{ \AA}^2$ ) and significantly exceed those for the Se–chalcogen pairs.

In order to explain the anomalously large Debye–Waller factors for Pb–Pb pairs, we initially assumed that the solid solutions can undergo a transition to a microcoherent state, for example, due to mechanical effects when the powders were ground or because the solid solution decomposes when the alloys are not cooled fast enough after annealing. In order to verify this proposition, a second series of samples was prepared with compositions identical to those in the first series. The alloys in this series were ground before annealing and all the annealed powders were quenched from  $720^\circ\text{C}$  in water. Data from these samples taken at the  $L_{\text{III}}$  absorption edge of Pb did not reveal any changes in the behavior of the Debye–Waller factor for the Pb–Pb pairs as a function of  $x$  compared to the first series of samples. Moreover, additional low-temperature annealing at  $100\text{--}400^\circ\text{C}$  was done on a

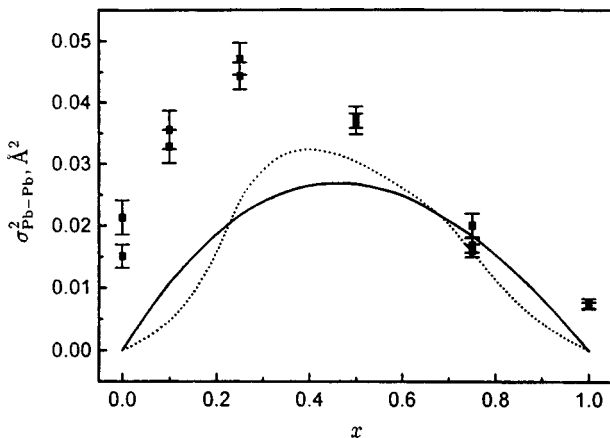


FIG. 6. The Debye–Waller factor for Pb–Pb atom pairs as a function of the composition  $x$  of  $\text{PbTe}_{1-x}\text{Se}_x$  solid solutions. The points are experimental data. The smooth curve was calculated by a Monte Carlo method and the dotted curve is the result of an analysis for the model  $\chi(k)$  curves.

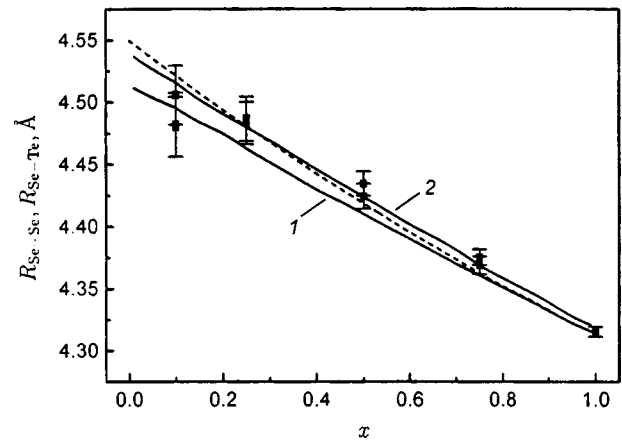


FIG. 7. The Se–Se (1) and Se–Te (2) interatomic distances as functions of the composition  $x$  of  $\text{PbTe}_{1-x}\text{Se}_x$  solid solutions. The points are experimental data. The smooth curves were calculated by a Monte Carlo method and the dashed curve is the average interatomic distance calculated from the lattice parameter.

number of samples from the second series with  $x=0.25$  in order to observe any changes caused by possible decomposition of the solid solution. No significant changes were observed in the Debye–Waller factor for the Pb–Pb pairs.

In order to understand the reason for the unusual behavior of the interatomic distances and Debye–Waller factor as functions of composition for the Pb–Pb pairs (Figs. 5 and 6), we decided to model the static distortions in the  $\text{PbTe}_{1-x}\text{Se}_x$  solid solutions by a Monte Carlo method. This method has been used previously<sup>3,15</sup> to model distortions in semiconductor solid solutions with a sphalerite structure.

### 3. MONTE CARLO MODEL

The static distortions in  $\text{PbTe}_{1-x}\text{Se}_x$  solid solutions were modelled in the approximation of elastically deformed bonds. For a given random distribution of Se and Te atoms in one of the fcc sublattices, a set of atomic coordinates  $\{\mathbf{r}_i\}$

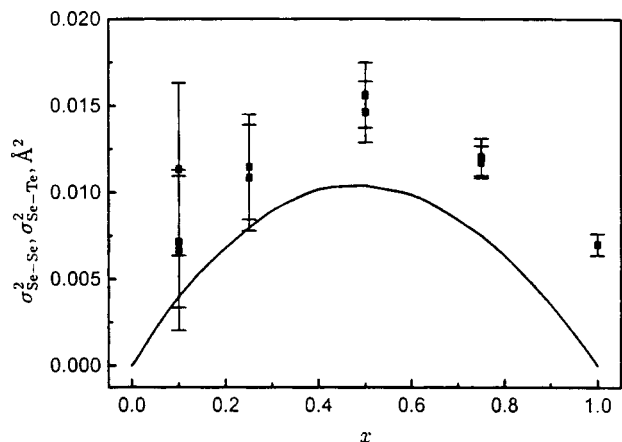


FIG. 8. The Debye–Waller factors for Se–Se and Se–Te atom pairs as functions of the composition  $x$  of  $\text{PbTe}_{1-x}\text{Se}_x$  solid solutions. The points are experimental data. The smooth curve was calculated by a Monte Carlo method.

was found for which the total strain energy from the change in the bond lengths and deviation of the angles between them from  $90^\circ$ ,

$$U = \frac{1}{2} \sum_i \left[ \sum_{j=1}^6 A_{s(i,j)} \left( \frac{|\mathbf{r}_i - \mathbf{r}_j| - d_{s(i,j)}}{d_{s(i,j)}} \right)^2 + B \sum_{(j,k)=1}^{12} \left( \frac{(\mathbf{r}_i - \mathbf{r}_j)(\mathbf{r}_i - \mathbf{r}_k)}{|\mathbf{r}_i - \mathbf{r}_j| |\mathbf{r}_i - \mathbf{r}_k|} \right)^2 \right],$$

was minimized. In the first term the sum is taken over the six nearest neighbors for each of the lattice sites. The indices  $s(i,j) = 1, 2$  correspond to Pb–Se and Pb–Te atom pairs at sites  $i$  and  $j$ ,  $A_s$  is the stiffness coefficient for the corresponding bond, and  $d_s$  is its equilibrium length in the binary compound ( $d_1 = 3.050$ ,  $d_2 = 3.217$  Å at 80 K). In the second term the sum is taken over all 12 different angles between bond pairs for each of the lattice sites. The stiffness constants with respect to lengthening of the Pb–Se ( $A_1$ ) and Pb–Te ( $A_2$ ) bonds were calculated from published<sup>16</sup> values of the elastic moduli for PbSe and PbTe according to the relation  $A = (C_{11} + 2C_{12})/4$ , and the stiffness constants with respect to bending, according to  $B = C_{44}/32$ , where  $C_{44}$  is the average of the corresponding moduli for PbSe and PbTe.

The model calculations were done on  $m \times m \times m$  lattices with  $m = 10 - 30$  nodes and periodic boundary conditions for several random distributions of the Se and Te atoms in the chalcogenide sublattice. Starting at a position among the nodes of an ideal fcc lattice, each of the atoms could undergo a shift in a direction for which the strain energy of the lattice decreased for a fixed position of the remaining atoms. The step size for a single displacement was adaptively reduced from 0.01 to 0.0002 Å. After roughly 1000 iteration steps per atom, the strain energy  $U$  ceased to vary and the resulting configuration of displacements was assumed to be in equilibrium. The set of coordinates for all the pairs of atoms located in the first- and second-coordination spheres found in this way was used to calculate the distribution function for the interatomic distances. Since the periodic boundary conditions required that the lattice parameter be fixed, the calculations were done for an entire set of these lattice parameters. In the following, we shall take the lattice parameter to be the value for which a minimum energy  $U$  was obtained.

Model calculations on lattices of different sizes showed that the excess energy owing to the finite lattice size varies roughly as  $m^{-3}$  and that for  $m > 16$ , finite lattice effects can be neglected.

The Monte Carlo calculations of the average Pb–Se and Pb–Te bond lengths and their dispersions (static Debye–Waller factors) as functions of  $x$  are plotted as the smooth curves in Figs. 3 and 4. As is to be expected, the distribution of the distances in the first-coordination sphere has a distinct bimodal character. We shall define the relaxation parameter  $\varepsilon'$  for the  $A-C$  bond as the change in the bond length for the extreme compositions of the solid solution  $AB_{1-x}C_x$  relative to the change in the average interatomic distance,

$$\varepsilon' = \frac{R_{Ac}^0 - R_{Ac}[AB]}{R_{AB}^0 - R_{Ac}^0},$$

where  $R_{AB}^0$  and  $R_{Ac}^0$  are the bond lengths in the binary compounds  $AB$  and  $AC$ , and  $R_{Ac}[AB]$  is the length of the  $A-C$  bond for impurity  $C$  in compound  $AB$  (in the limit of infinite dilution). For the Pb–Te and Pb–Se bonds, this quantity was 0.35 and 0.21, respectively. The difference between the two values of  $\varepsilon'$  is a consequence of the substantial difference between the stiffness coefficients  $A_1$  and  $A_2$  (roughly a factor of 1.5). The value of  $\varepsilon'$  calculated for the Pb–Te bond is in fair agreement with experiment ( $\varepsilon' \approx 0.36$ ). A comparison for the Pb–Se bond is difficult because of the large experimental errors. It is interesting that the calculations of the average interatomic distance as a function of composition (the dashed curve in Fig. 3) deviate significantly (by roughly 0.009 Å) and negatively from Vegard's law.

Figures 5–8 contain plots of the average interatomic distances and their dispersions for Pb–Pb, Se–Se, and Se–Te atom pairs in the second-coordination sphere with respect to one another. The substantially larger static Debye–Waller factors for the second-coordination sphere compared to the first mean that the lattice adapts to the existence of different chemical bond lengths through local rotation. The model results for Se–chalcogen atom pairs are in fairly good agreement with experimental data, while the results for Pb–Pb pairs are in poor agreement with experiment. The reasons for this discrepancy will be discussed in detail in the next section.

According to our model calculations, the average Se–Se distance in the solid solution is 0.01–0.02 Å shorter than the Se–Te distance (Fig. 7) and their Debye–Waller factors are roughly equal ( $\sigma_{Se-Se}^2 \approx \sigma_{Se-Te}^2$ ). This justifies treating the chalcogenide atoms as a single second-coordination sphere during the analysis of the surroundings of the selenium atoms.

Therefore, Monte Carlo modelling of the distortions in  $PbTe_{1-x}Se_x$  solid solutions has made it possible to establish the inevitability of strong static distortions in the Pb–Pb distance and to demonstrate qualitative agreement between the calculations and experiment for the first-coordination sphere and for the Se–chalcogenide atom pairs. The model calculations, however, have not provided an explanation for the discrepancy between the experimentally determined and calculated Pb–Pb distances, which may be related to an inadequacy of the one-dimensional approximation employed to analyze the experimental data for the Pb–Pb distances.

#### 4. DISCUSSION

We now discuss the validity of a single-mode approximation for the interatomic distances in the second-coordination sphere of  $PbTe_{1-x}Se_x$  solid solutions.

It has been proposed<sup>1,17</sup> that the number of “modes” in the distribution of the  $A-A$  distances in an  $AB_{1-x}C_x$  solid solution is determined by the number of different combinations through which a pair of  $A$  atoms are bound, i.e., the distribution must be bimodal for lattices having a sphalerite structure and trimodal for NaCl-type lattices.

Thus, in processing our experimental data, we have begun with an attempt to find a set of parameters with which the distribution of the Pb–Pb distances could be represented

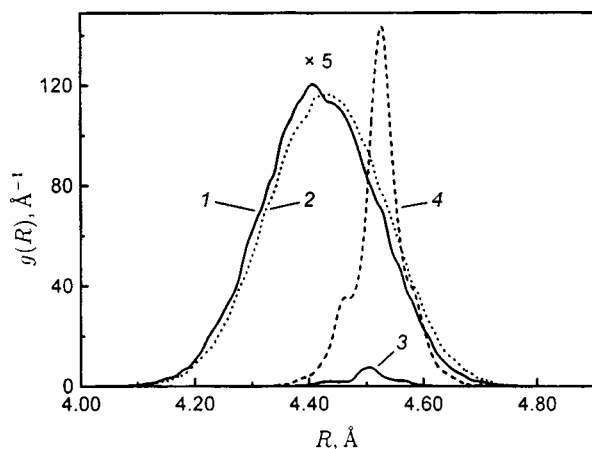


FIG. 9. Distributions of the Se–Se (1, 3) and Se–Te (2, 4) interatomic distances for  $\text{PbTe}_{1-x}\text{Se}_x$  samples with  $x=0.5$  (1, 2) and  $x=0.05$  (3, 4), calculated by a Monte Carlo method.

in the form of a sum of several Gaussians. Unfortunately, because of the large Debye–Waller factor for Pb–Pb pairs, the range of data in  $k$  space within which the EXAFS oscillations were observed was limited and did not allow us to determine the parameters for a trimodal model (the solution was unstable). In the bimodal approximation, physically reasonable values of the distances could be obtained only for compositions close to the binary compounds; near  $x=0.5$  the distance to one of the components of the coordination sphere became unphysically large ( $\sim 4.7$  Å). Since neither the trimodal nor the bimodal description could be used for processing the data from all the samples, we were forced to limit the analysis to the single-mode approximation.

Let us consider the distribution functions  $g(R)$  for Se–Se, Se–Te and Pb–Pb atom pairs calculated by a Monte Carlo method (Figs. 9 and 10). It is clear that for  $x \approx 0$  and  $x \approx 1$ , the distribution functions have a fine structure, which is smeared out as  $x \rightarrow 0.5$ . The difference between the distribution functions for Se–chalcogenide and Pb–Pb atom pairs is the following: for the surroundings of selenium (Fig. 9), the average Se–Se and Se–Te interatomic distances are close

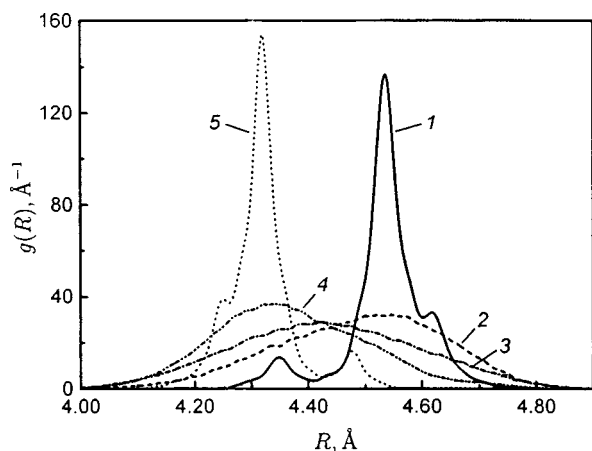


FIG. 10. Distributions of the Pb–Pb interatomic distances for  $\text{PbTe}_{1-x}\text{Se}_x$  samples with different compositions calculated by a Monte-Carlo method.  $x$ : 1 — 0.05, 2 — 0.25, 3 — 0.5, 4 — 0.75, 5 — 0.95.

and the fine structure components are relatively close to one another, at distances of the order of the amplitude of the thermal vibrations at 80 K. For the surroundings of lead (Fig. 10), on the other hand, a rather sharply expressed structure is typical, with distances between the components that greatly exceed the amplitude of the thermal vibrations. These results confirm the general phenomenon<sup>1,6</sup> that the distribution of the distances between the atoms which undergo substitution in the solid solution  $AB_{1-x}C_x$  can be regarded as having a single mode, while for atom pairs A–A, it is more complicated.

Figure 10 implies that the distribution function for atom pairs A–A in our solid solution with an NaCl structure cannot be described in the trimodal approximation. Nevertheless, the fine structure components can be divided arbitrarily into two groups whose centers of gravity differ significantly. Therefore, it appears that, when the smearing of the curves is not too great, it is possible to approximate the distribution function by a sum of two Gaussians.

In order to check how well the Monte Carlo calculations of the distribution functions agree with the experimental data, we have used the functions  $g(R)$  found here to compute  $\chi(k)$  according to

$$\chi(k) = \frac{S_0^2}{k} f(k) \int \frac{g(R)}{R^2} \exp[-2R/\lambda(k)] \sin[2kR + \psi(k)] dR.$$

Then the synthesized curves were processed by the same method employed for the experimental data (one distance in the second-ordination sphere). The interatomic distances and static Debye–Waller factors found in this way are plotted as dotted curves in Figs. 5 and 6. The resulting curves are in good agreement with the experimental data, i.e., the Monte Carlo calculations of the distribution function provide a qualitatively accurate description of the actual structure of the solid solution.

Our results, therefore, show that the distortions in the second-ordination sphere of atoms in the chalcogenide sublattice in  $\text{PbTe}_{1-x}\text{Se}_x$  solid solutions (where substitution takes place) can be described with sufficient accuracy in a single-mode approximation while, for the atoms in the lead sublattice (not subject to substitution), it is difficult to find a good working approximation and the best way out is to use distribution functions calculated by a Monte Carlo method.

The experimentally measured Debye–Waller factors are known to consist of static and dynamic terms which correspond to static distortions of the structure and thermal lattice vibrations. A Monte Carlo calculation only gives the static part of the Debye–Waller factor. Thus, the observed discrepancy between the experimental and calculated Debye–Waller factors can be attributed to thermal vibrations. In the first coordination sphere (Fig. 4), the dynamic contribution to the Debye–Waller factor is an order of magnitude greater than the static contribution, even at 80 K. The difference in the factors for Pb–Te and Pb–Se bonds appears to be related to the substantial mass difference between tellurium and selenium atoms. A more detailed analysis of these data becomes difficult because the phonon spectrum in  $\text{PbTe}_{1-x}\text{Se}_x$  is

bimodal.<sup>18</sup> The contribution of thermal vibrations to the Debye–Waller factor for Se–chalcogenide atom pairs (Fig. 8) turns out to be slightly greater for the atoms in the first-coordination sphere (the movements of the atoms in the second-coordination sphere are more weakly correlated) and the measurements are independent of  $x$  to within the measurement error. However, as Fig. 6 implies, for Pb–Pb atom pairs, the thermal contribution depends on  $x$ . The maximum amplitude of the thermal vibrations is observed at  $x \approx 0.25$ . This result is qualitatively consistent with our earlier data,<sup>11</sup> and this implies that the lattice of the  $\text{PbTe}_{1-x}\text{Se}_x$  solid solution with  $x \approx 0.25$  is “softer,” so that a phase transition can be observed when part of the lead atoms are replaced by tin.

We now consider the features of the local structure of  $\text{PbTe}_{1-x}\text{Se}_x$  solid solutions. As shown above, the parameter  $\varepsilon'$  was  $\approx 0.36$  for this solid solution, i.e., it is intermediate between the values observed previously in III–V and II–VI semiconductors with a sphalerite structure<sup>5</sup> (0.05–0.24) and in alkali halide crystals with an NaCl structure<sup>17</sup> ( $\approx 0.5$ ).

It is obvious that one of the main factors leading to changes in the bond length around an impurity atom is the appearance of elastic deformations caused by the difference in size of the substituted atoms  $B$  and  $C$ . As simple arguments show,<sup>19</sup>  $\varepsilon'$  is determined by the crystal structure (mutual position of the atoms in the lattice), so that it is only meaningful to compare data obtained for identical structures. Neglecting bond bending and displacement of atoms in the second- and further-coordination spheres with the same stiffness for  $A$ – $B$  and  $A$ – $C$  bonds,  $\varepsilon' = 0.25$  was found for a sphalerite structure and  $\varepsilon' = 0.5$  for an NaCl structure. The more realistic Monte Carlo calculation done here, which took the influence of all the factors listed above into account, yielded  $\varepsilon' = 0.35$  and  $0.21$  for the two bonds in a  $\text{PbTe}_{1-x}\text{Se}_x$  solid solution with an NaCl structure, which is in fair agreement with experiment.

However, the strain contribution, alone, appears to be insufficient to explain all the experimental data. An attempt<sup>17</sup> to calculate  $\varepsilon'$  by a Monte Carlo method for the alkali halide  $\text{RbBr}_{1-x}\text{I}_x$  and  $\text{K}_{1-x}\text{Rb}_x\text{Br}$  crystals with an NaCl structure yielded values close to those found for  $\text{PbTe}_{1-x}\text{Se}_x$ , but differing substantially from experiment. A large difference between experimental values of  $\varepsilon'$  for III–V and II–VI semiconductors with a sphalerite structure and those predicted by the deformation model has also been noticed.<sup>5</sup> We believe that these discrepancies are associated with another group of factors which can affect the local structure, namely, the so-called chemical factors, which take into account the individual properties of the interacting atoms (their valence, electronegativity) and chemical bond type.

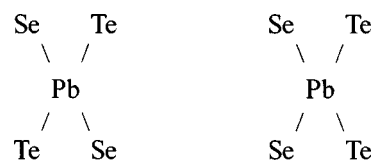
These factors also show up in the thermodynamic properties; thus, the enthalpy of mixing a solid solution,  $\Delta H_m$ , is known to consist of two components, strain and chemical. The total deformation energy  $U$  calculated by a Monte Carlo method is just the strain contribution to  $\Delta H_m$ . In III–V and II–VI semiconductors with a sphalerite structure, the strain energy is in good agreement with the experimentally determined enthalpy of mixing.<sup>20</sup> Unfortunately, the available published data on the enthalpy of mixing of  $\text{PbTe}_{1-x}\text{Se}_x$  solid solutions ( $\Delta H_m \leq 0.2$  kcal/mole) are not very exact.

And, although this quantity is positive, which is indicative of a potential tendency for the solid solution to decompose, the difference between the calculated strain term ( $U = 0.38$  kcal/mole) and the measured  $\Delta H_m$  may be evidence of the presence of chemical factors.

Individual members of this group of factors may either increase or reduce  $\varepsilon'$  (the chemical bond length). Let us assume that in the solid solution under study here, their effects are compensated and the agreement between the calculated and experimental  $\varepsilon'$  is good.

The local concentrations of Se–Se (short-term order) found in our experiments can be used to estimate the contribution of chemical factors to the enthalpy of mixing. We shall take the temperature  $T_f$  at which the diffusion of the chalcogenide atoms freezes out to be the temperature at which two nearest chalcogenide atoms undergo exchange in one second, which corresponds to a diffusion coefficient of  $D = 2 \cdot 10^{-15}$  cm<sup>2</sup>/s. The known<sup>21</sup> temperature variations of the diffusion coefficients yield an estimate of  $T_f \approx 540$  K and, in the approximation of a pairwise interatomic interaction, we have calculated how much greater the energy of an Se–Te pair is than the average energy of the Se–Se and Te–Te pairs:  $\Delta E \approx 0.5$  kcal/mole (0.02 eV) for a sample with  $x = 0.5$ . This value gives an idea of the magnitude of the chemical contribution to the enthalpy of mixing, since atoms in the second-coordination sphere do not interact through deformations, so there is no strain contribution to this quantity. A comparison of the values of  $\Delta E$  and  $U$  obtained here shows that in the  $\text{PbTe}_{1-x}\text{Se}_x$  solid solutions the strain and chemical contributions to the enthalpy of mixing are of the same order of magnitude.

The use of a pairwise interatomic-interaction approximation is not, however, entirely correct, since the atoms in the second-coordination sphere do not interact directly (either chemically or deformationally). The development of short-range order is apparently associated with some sort of more complicated interactions involving three or more atoms. In our experiments, the largest deviations from a statistical distribution of the chalcogenide atoms were observed at low Se concentrations and showed up as an elevated number of Se–Pb–Se configurations with 90° Pb–Se bonds. This suggests that there is a significant difference in the energies of the configurations in which atoms of given species lie in the same and in different  $p$  orbitals. These configurations can be represented schematically in the following way:



It is not impossible that this behavior originates in peculiarities of the chemical bond in IV–VI semiconductors, specifically its unsaturated character.

Using the strain approximation for calculating the bond lengths and pairwise distribution functions in the first- and second-coordination spheres, therefore, provides a qualitatively accurate description of the distortion in the structure of

PbTe<sub>1-x</sub>Se<sub>x</sub> solid solutions. However, this model cannot explain the differences in the experimentally observed  $\varepsilon'$  in systems for which the model predicts close values of that parameter as well as the development of short-range order. This indicates that chemical factors must be taken into account, along with the deformation interaction, when describing the properties of solid solutions.

This work was supported by the Russian Fund for Fundamental Research (Grant No. 95-02-04644).

<sup>a)</sup>Studies of solid solutions with a sphalerite structure<sup>1-3</sup> have shown that the atoms in the second-coordination sphere can also be at different distances. Our assumption will be justified below.

<sup>b)</sup>To determine the parameters more accurately the additional assumptions  $R_{\text{Se-Te}} = R_{\text{Se-Se}}$  and  $\sigma_{\text{Se-Te}}^2 = \sigma_{\text{Se-Se}}^2$  were introduced, and the Te and Se atoms were treated as a single-coordination sphere. These restrictions are justified by earlier studies of solid solutions which revealed a single-mode distribution of the bond lengths in the solid solution sublattice, within which isoelectronic substitution takes place,<sup>1,6</sup> and by our Monte Carlo modelling of the structure of the PbTe<sub>1-x</sub>Se<sub>x</sub> solid solution. (See the next section.)

<sup>c)</sup>In analyzing the data we have included the systematic errors in calculating the theoretical scattering amplitudes and phases using the FEFF program. The distances obtained at the Pb edge were corrected by 0.025 Å,<sup>10</sup> and in analyzing the data obtained at the Se edge, a statistical correction of 0.5 rad was added to the scattering phase. These corrections ensured good agreement between the distances obtained by processing the EXAFS spectra and from x-ray data for standard PbTe and PbSe compounds.

<sup>1</sup>J. C. Mikkelsen, Jr. and J. B. Boice, Phys. Rev. B **28**, 7130 (1983).

<sup>2</sup>A. Balzarotti, N. Motta, A. Kisiel, M. Zimnal-Starnawska, M. T. Czyżyk, and M. Podgórnny, Phys. Rev. B **31**, 7526 (1985).

<sup>3</sup>N. Motta, A. Balzarotti, P. Letardi, A. Kisiel, M. T. Czyżyk, M. Zimnal-Starnawska, and M. Podgórnny, Solid State Commun. **53**, 509 (1985).

<sup>4</sup>W.-E. Pong, R. A. Mayanovic, B. A. Bunker, J. K. Furdyna, and U. Debska, Phys. Rev. B **41**, 8440 (1990).

<sup>5</sup>R. A. Mayanovic, W.-E. Pong, and B. A. Bunker, Phys. Rev. B **42**, 11174 (1990).

<sup>6</sup>Z. H. Wu, K. Q. Lu, Y. R. Wang, J. Dong, H. F. Li, C. X. Li, and Z. Z. Fang, Phys. Rev. B **48**, 8694 (1993).

<sup>7</sup>Q. Islam and B. A. Bunker, Phys. Rev. Lett. **59**, 2701 (1987).

<sup>8</sup>B. A. Bunker, Q. T. Islam, and W. F. Pong, Physica B **158**, 578 (1989).

<sup>9</sup>Z. Wang and B. A. Bunker, Phys. Rev. B **46**, 11277 (1992).

<sup>10</sup>A. I. Lebedev, I. A. Sluchinskaya, V. N. Demin, and I. H. Munro, Phys. Rev. B **55**, 14770 (1997).

<sup>11</sup>A. I. Lebedev and I. A. Sluchinskaya, Fiz. Tverd. Tela (Leningrad) **32**, 1780 (1990) [Sov. Phys. Solid State **32**, 1036 (1990)].

<sup>12</sup>P. A. Lee, P. H. Citrin, P. Eisenberger, and B. M. Kincaid, Rev. Mod. Phys. **53**, 769 (1981).

<sup>13</sup>J. Mustre de Leon, J. J. Rehr, S. I. Zabinsky, and R. C. Albers, Phys. Rev. B **44**, 4146 (1991).

<sup>14</sup>Shamsuddin and S. Misra, Z. Metallkd. **70**, 541 (1979).

<sup>15</sup>M. Podgórnny, M. T. Czyżyk, A. Balzarotti, P. Letardi, N. Motta, A. Kisiel, and M. Zimnal-Starnawska, Solid State Commun. **55**, 413 (1985).

<sup>16</sup>*Numerical Data and Functional Relationships in Science and Technology*, Landolt-Börnstein New Series, Group 3, Vol. 17f (Springer-Verlag, Berlin, 1983).

<sup>17</sup>J. B. Boyce and J. C. Mikkelsen, Jr., Phys. Rev. B **31**, 6903 (1985).

<sup>18</sup>H. Finkenrath, G. Franz, and N. Uhle, Phys. Status Solidi B **95**, 179 (1979).

<sup>19</sup>C. K. Shih, W. E. Spicer, W. A. Harrison, and A. Sher, Phys. Rev. B **31**, 1139 (1985).

<sup>20</sup>Z. H. Wu and K. Q. Lu, J. Phys.: Condens. Matter **6**, 4437 (1994).

<sup>21</sup>*Numerical Data and Functional Relationships in Science and Technology*, Landolt-Börnstein New Series, Group 3, Vol. 17d (Springer-Verlag, Berlin, 1984).

Translated by D. H. McNeill